J. Phys. B: At. Mol. Opt. Phys. 26 (1993) 705-721. Printed in the UK

State selectivity in H^+–Na(3s/3p) collisions: differential cross sections, alignment and orientation effects for electron capture

A Dubois†, S E Nielsen‡ and J P Hansen§

† Laboratoire de Chimie Physique‖, Université Pierre et Marie Curie, 11, rue Pierre et Marie Curie, F-75231 Paris Cedex 05, France

‡ Department of Chemistry, H C Ørsted Institute, University of Copenhagen, DK-2100 Copenhagen Ø, Denmark

§ Institute of Physics, University of Bergen, Allegt. 55, N-5007 Bergen, Norway

Received 26 June 1992

Abstract. We present a theoretical study of state selectivity for electronic processes occurring in the course of collisions between ions and atoms. This analysis is performed within the semiclassical atomic basis impact parameter treatment in combination with the eikonal method to obtain angular differential cross sections and alignment and orientation parameters. We apply the formalism to H^+–Na collisions in the 0.75–5.0 keV energy range for which new experimental data are available, cf the companion paper and the comparison there with our theoretical predictions. We report and discuss the orientation of the final H(2p) and H(3p) capture states for an initial Na(3s) state and for initially oriented $Na(3p_{\pm 1})$ states.

1. Introduction

In the course of binary collisions between atomic species, different electronic processes can be activated on each centre by the interaction due to the other partner. The selectivity of the processes with respect to impact energies is well described by total cross sections. However, these quantities do not allow the analysis of the spatial selectivity. This is taken into account by angular differential analysis which provides a much sharper probe of process mechanisms and reveals collision dynamics.

The ultimate level of investigation is the unfolding of the magnetic state degeneracy by analysing the polarization of the fluorescence light of the excited atom. The coherence studies of orientation and alignment (cf review of Andersen *et al* 1988) allow confrontations between theory and experiment at the level of scattering amplitudes. Such sophisticated investigations require detection of heavy particles and photons in coincidence and the time-inverse type of experiment has often been preferred. A particular excited magnetic state is prepared by optical pumping with polarized laser light before the collision and the study of a specific electronic transition is carried out as a function of the orientation and alignment characteristics of this initial state (e.g. Campbell *et al* 1988).

The goal of this paper is to cover these three levels of information which can be obtained by present-day experimental techniques. With this intention we choose the H^+–Na collision system and focus on the study of the dominant $H(n=2)$ electron capture channels from initial Na(3s) and Na(3p) states.

‖ Unité de Recherche Associée au CNRS, URA 176.

0953-4075/93/040705+17$07.50

The H^+-Na system has already been the object of numerous experimental and theoretical studies, reporting especially total cross section results. Most of the experimental studies report total capture cross sections for H^+-Na(3s) collisions, e.g. Aumayr *et al* (1987) and references therein. The cross sections for capture into the complete $H(n=2)$ shell have been studied by time-of-flight techniques (Royer *et al* 1988). Specific cross sections for capture to the H(2s) state have been reported by Berkowitz and Zorn (1984), for H(2p) capture (L_α emission cross sections) by Finck *et al* (1988) and recently by Gieler *et al* (1991) in the (0.1-20) keV energy range. Application of tunable lasers has also allowed the study of electron capture in H^+-Na(3p) collisions. For the total $H(n=2)$ capture channels Dowek *et al* (1990) have analysed the effects of initial alignment of the Na(3p) states. Very recently these studies have been extended to differential measurements to analyse the effects of initial orientation of the Na(3p) states (Houver *et al* 1992). Richter *et al* (1993), in the following paper, report a complete density matrix determination of the $H^+ + Na(3p) \rightarrow H(n=2) + Na^+$ process. A study of initial orientation effects has also been undertaken by Roller-Lutz *et al* (1991) for $H^+ + Na(3p) \rightarrow H(2p) + Na^+$ transitions.

From the theoretical side, numerous integral cross sections for capture from the Na ground state have been published and in general excellent agreement has been achieved: in atomic-orbital closed-coupling calculations (e.g. Fritsch 1984, Shingal and Bransden 1987, Dubois *et al* 1991) and in molecular-orbital close-coupling calculations (Courbin *et al* 1990). For capture from Na(3p), much fewer calculations have been carried out: in the AO basis by Fritsch (1990) and in the MO basis by Allan *et al* (1990). Recent classical trajectory Monte Carlo studies of orientation effects in this system have been published by Lewartowski and Courbin (1992).

In section 2 we present the theoretical framework of our study: the semiclassical atomic-basis model and the eikonal method to obtain angular differential cross sections. More specifically we emphasize the derivation of the scattering amplitudes for transitions between states which do not have cylindrical collision symmetry. Section 3 is devoted to the study of H^+-Na collisions: we first present integral cross sections in comparison with previously reported results and secondly, orientation and alignment effects for specific initial and final states are illustrated by differential cross section results. The comparison with experiments is presented in the companion paper by Richter *et al* (1993). A short conclusion on present and future extensions of this study and perspectives for possible experiments ends the paper.

2. Theory

2.1. Eikonal method scattering amplitudes

We have based our calculations of differential cross sections for excitation and capture processes, involving aligned and oriented states, on the eikonal method. A systematic quantal description of scattering amplitudes in medium to high energy atomic collisions was first formulated by McCarroll and Salin (1968) for s-s capture in a two-state impact parameter treatment and by Wilets and Wallace (1968) in terms of Fraunhofer integrals over classical trajectory amplitudes. Later Flannery and McCann (1973) derived and discussed successive approximations within the eikonal method using a multistate impact parameter treatment of excitation in heavy particle collisions. A useful introduction to the approach, including capture channels as well, has been given

by McCarroll (1982) and most recently by Briggs and Macek (1990) in a survey of high energy ion–atom collisions.

We shall not go through the details of the derivation of the eikonal method results but refer to the references given above. However, we shall present scattering amplitude expressions for excitation and capture channels and point out some important phase features, particularly of relevance for differential predictions in collisions involving aligned and oriented atomic states.

In the stationary scattering formulation the centre-of-mass scattering amplitudes for quasi-one-electron systems, e.g. H^+–Na, may be expressed (in au)

$$f_{fi}(\Omega) = -\frac{\mu_f}{2\pi}\langle \Phi_f(\boldsymbol{k}_f, \boldsymbol{r}, \boldsymbol{R})|\, V_f(\boldsymbol{r}, \boldsymbol{R})|\Psi^+_{(i)}(\boldsymbol{k}_i, \boldsymbol{r}, \boldsymbol{R})\rangle \tag{2.1}$$

where the angles $\Omega = (\theta, \phi)$ are the spherical angles of the final momentum vector $\boldsymbol{k}_f$, for capture here H relative to Na^+, and the quantization axis is along the initial momentum vector $\boldsymbol{k}_i$, i.e. $\boldsymbol{k}_i = k_i\hat{Z} = \mu v\hat{Z}$, cf figure 1. $V_f(\boldsymbol{r}, \boldsymbol{R})$ is the final channel electrostatic interaction (here between the separated atoms H and Na^+), μ_f is the final channel reduced mass, Φ_f is the final stationary scattering state of the separated atoms

$$\Phi_f(\boldsymbol{k}_f, \boldsymbol{r}, \boldsymbol{R}) = e^{-i\boldsymbol{k}_f\cdot\boldsymbol{R}_B}\phi^B_f(\boldsymbol{r}_B) \tag{2.2}$$

and $\Psi^+_{(i)}$ the full solution of the time-independent Schrödinger equation, subject to the asymptotic boundary conditions,

$$\Psi^+_{(i)} \xrightarrow[R_A\to\infty]{} \sum_n \left[e^{i\boldsymbol{k}_n\cdot\boldsymbol{R}_A}\delta_{n,i} + f_{in}(\Omega)\frac{e^{ik_nR_A}}{R_A}\right]\phi^A_n(\boldsymbol{r}_A) \tag{2.3a}$$

$$\xrightarrow[R_B\to\infty]{} \sum_m \left[f_{im}(\Omega)\frac{e^{ik_mR_B}}{R_B}\right]\phi^B_m(\boldsymbol{r}_B). \tag{2.3b}$$

Assuming a full solution of the Schrödinger equation in the form $\Psi^+_{(i)} = e^{i\boldsymbol{k}_i\cdot\boldsymbol{R}_A}\psi_{(i)}(\boldsymbol{r}, \boldsymbol{R})$, neglecting in the eikonal method second-order derivatives $\nabla^2_R\psi_{(i)}$, and

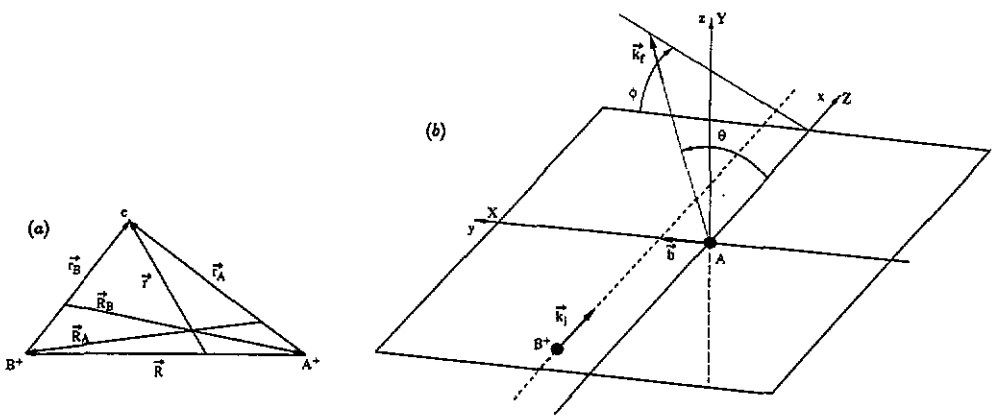

Figure 1. (*a*) Position vector for the quasi-one-electron ion–atom system. (*b*) Left-hand side projectile straight line trajectory and detection geometry. The two reference frames used in this paper: the *XYZ* frame with the *Z* axis along the initial momentum vector $\boldsymbol{k}_i$ of the projectile, in which the states have the convenient cylindrical collision symmetry, the *xyz* frame with the *x* axis along $\boldsymbol{k}_i$ and the quantization axis *z* perpendicular to $\boldsymbol{k}_i$ and coinciding with a laser beam direction and/or photon detection direction. The momentum vector $\boldsymbol{k}_f$ of the projectile after scattering is defined by the angles (θ, ϕ).

identifying $\boldsymbol{R}$ with a constant-velocity heavy-particle trajectory, $\boldsymbol{R} = \boldsymbol{b} + \boldsymbol{v}t$, leads to the usual time-dependent Schrödinger equation, $[H_{el} - i\partial/\partial t]\psi'_{(i)}(r, \boldsymbol{R}(t)) = 0$, for the electronic state $\psi'_{(i)} = \psi_{(i)}\, e^{-i\epsilon_{(i)}^{\hat{A}}t}$. The scattering amplitude for capture may now be expressed (up to first order terms in the electron mass over nuclear mass) as the following integral over the cylindrical coordinates of $\boldsymbol{R}(b, \Phi, Z)$

$$f_{fi}(\Omega) = -\frac{\mu_f}{2\pi}\int_0^{\infty} b\,db\int_0^{2\pi} d\Phi\int_{-\infty}^{+\infty} dZ\, e^{-i\boldsymbol{k}_{f\perp}\cdot\boldsymbol{b}} \times (e^{i(\varepsilon_f^B + \frac{1}{2}v^2)Z/v}\langle\phi_f^B|V_f\, e^{-iv\cdot r_A}|\psi'_{(i)}\rangle) \tag{2.4}$$

where $\boldsymbol{k}_{f\perp}$ is the $\boldsymbol{k}_f$ projection on the (b, Φ) plane perpendicular to $\boldsymbol{k}_i$. The electronic state $\psi'_{(i)}$ represented by the ETF (electron translational factor) modified atomic expansion, choosing for convenience the origin at the target nucleus A,

$$\psi'_{(i)}(r, b, \Phi, Z) = \sum_n c_n^A(b, \Phi, Z)\phi_n^A(r_A)\, e^{-i\varepsilon_n^A Z/v} + \sum_m c_m^B(b, \Phi, Z)\phi_m^B(r_B)\, e^{iv\cdot r_A}\, e^{-i(\varepsilon_m^B + \frac{1}{2}v^2)Z/v} \tag{2.5}$$

with initial conditions $c_n^A(b, \Phi, -\infty) = \delta_{n,i}$ and $c_m^B(b, \Phi, -\infty) = 0$, may be obtained from the impact parameter solution of the time-dependent Schrödinger equation in the ZX plane with $\Phi = 0$, $c_j^{A,B}(b, Z)$ since

$$c_j^{A,B}(b, \Phi, Z) = c_j^{A,B}(b, Z)\, e^{-i(m_j - m_i)\Phi} \tag{2.6}$$

due to the cylindrical collision symmetry of the atomic states in the XYZ frame, m_i and m_f being the initial and final magnetic quantum numbers with respect to the Z axis.

Finally using the unitarity of the close-coupling impact parameter solution and the complete form of the close-coupled equations for the collision amplitudes $c_n^{A,B}(b, Z)$ we find that we may replace the bracketed part of the integrand in (2.4) by $iv(\partial/\partial Z)[c_f^B(b, \Phi, Z) + \Sigma_n \langle\phi_f^B|e^{-iv\cdot r_A}|\phi_n^A\rangle\, e^{i(\varepsilon_f^B + v^2/2 - \varepsilon_n^A)Z/v} c_n^A(b, \Phi, Z)]$. Thus the Z integration in (2.4) may be performed exactly and, using the initial conditions and the vanishing of the overlap matrix at infinity, leads to the scattering amplitude for capture,

$$f_{fi}(\Omega) = -\frac{i\mu_f v}{2\pi}\int_0^{\infty} b\,db\int_0^{2\pi} d\Phi\, e^{-i[k_{f\perp}\cdot b + (m_f - m_i)\Phi]}[c_f^{(i)}(b, +\infty) - \delta_{f,i}] \tag{2.7}$$

completely identical in form to the expression for the scattering amplitude for excitation. For that reason we have left out in equation (2.7) specific references to the orbital centres of the electron before and after collision, but rather specified by the index i the particular initial condition chosen for the target state in the close-coupling solution of the impact parameter equations, $c_f^{(i)}(b, Z)$, and the final state index f may refer to the elastic, inelastic as well as the electron transfer amplitudes. For small angle scattering and small energy defects compared to the collision energy we may express the dot product of $\boldsymbol{b}$ and the final momentum perpendicular to the z axis as

$$\boldsymbol{k}_{f\perp}\cdot\boldsymbol{b} \simeq \eta b\cos(\phi - \Phi) \qquad \eta = 2\mu v\sin(\theta/2) \simeq \mu v\theta \tag{2.8}$$

and when introduced into (2.7) the Φ-integration can be performed analytically to give the scattering amplitude as a Bessel function transform of the collision amplitude,

$$f_{fi}(\theta, \phi) = \mu v(-i)^{1+|m_f - m_i|}\, e^{-i(m_f - m_i)\phi}\int_0^{\infty} b\,db J_{|m_f - m_i|}(\eta b)[c_f^{(i)}(b, +\infty) - \delta_{f,i}]. \tag{2.9}$$

This expression agrees with that of Wilets and Wallace (1968) for the special case $m_i = 0$ but, however, shows an additional phase of $(-1)^{|m_f - m_i|}$ compared to the expression given by Flannery and McCann (1973). The phase factor is of no importance for the differential cross sections related to the excitation and capture states quantized in the XYZ frame of reference. However, as we shall see in the following, the correct phase of the expression (2.9) will be decisive for the scattering amplitudes and the differential cross sections related to aligned and oriented initial and final atomic states in the xyz frame. It is well known that all b-dependent phases contributing to the collision amplitudes $c_f^{(i)}(b, +\infty)$ in the complete solution of the close-coupled impact parameter equations should be included in the integrand of (2.9), common phases due to the core-core interaction in the Hamiltonian, and long range Coulomb phases associated with the particular channels (Piacentini and Salin 1977). It is precisely the complete phase information that allows the extraction of the angular predictions from straight-line trajectory collision amplitudes. Explicitly,

$$c_f^{(i)}(b, +\infty) = a_f^{(i)}(b, Z_0) \exp\left(\frac{\mathrm{i}}{v}\left[2Z^{\mathrm{A}}Z^{\mathrm{B}} \ln b - (Z^{\mathrm{B}} + Z^f) \ln(\sqrt{Z_0^2 + b^2} + Z_0)\right]\right) \tag{2.10}$$

where $a_f^{(i)}(b, Z_0)$ is the solution of the close-coupled impact parameter equations without the core-core interaction, starting (initial conditions) at $-Z_0$ along the projectile trajectory and ending at $+Z_0$ for the usual left-side passage of the target ($\Phi = 0$), cf figure 1, and Z^{A}, Z^{B} and Z^f are the core charges of the target, the projectile and the final orbital core (B for excitation and A for capture), respectively.

2.2. Scattering amplitudes for oriented states in the xyz frame

We shall consider next the scattering off target states quantized (oriented) with respect to a z axis perpendicular to the projectile beam direction and coinciding with a laser beam direction, and/or the photon detection direction. In this frame of reference, the projectile beam direction defines the x axis ($x = Z$) and $z = Y$, cf figure 1.

Scattering amplitudes (indicated by $\perp$ superscript) for initial and final states quantized in this xyz frame of reference may now be obtained as linear combinations of the scattering amplitudes for initial and final states in the XYZ scattering frame, equation (2.9). For s-p processes, we obtain

$$f^{\perp}_{\mathrm{p}_{\pm 1}\mathrm{s}}(\theta, \phi) = \mp\frac{1}{\sqrt{2}} f_{\mathrm{p}_0\mathrm{s}} + \frac{\mathrm{i}}{2}(f_{\mathrm{p}_{-1}\mathrm{s}} - f_{\mathrm{p}_{+1}\mathrm{s}}) \tag{2.11a}$$

$$= \mathrm{i}\mu v \int_0^\infty b\, \mathrm{d}b \left[\pm\frac{1}{\sqrt{2}} J_0(\eta b) c^{(s)}_{\mathrm{p}_0}(b, +\infty) + \cos\phi J_1(\eta b) c^{(s)}_{\mathrm{p}_1}(b, +\infty)\right]$$

$$= \pm\frac{1}{\sqrt{2}} T^{(s)}_{\mathrm{p}_0}(\theta) + \cos\phi T^{(s)}_{\mathrm{p}_1}(\theta) \tag{2.11b}$$

$$f^{\perp}_{\mathrm{p}_0\mathrm{s}}(\theta, \phi) = -\frac{\mathrm{i}}{\sqrt{2}}(f_{\mathrm{p}_{+1}\mathrm{s}} + f_{\mathrm{p}_{-1}\mathrm{s}}) = -\mathrm{i}\sqrt{2} \sin\phi T^{(s)}_{\mathrm{p}_1}(\theta) \tag{2.12}$$

introducing a short-hand notation for the Bessel transform

$$T_f^{(i)}(\theta) \equiv \mathrm{i}\mu v \int_0^\infty b\, \mathrm{d}b\, J_{|m_f - m_i|}(\eta b) c_f^{(i)}(b, +\infty). \tag{2.13}$$

Left-hand/right-hand differential scattering asymmetry for final oriented p states follows directly from the scattering amplitudes (2.11*b*), i.e. $f^{\perp}_{p_{+1}s}(\theta, \phi) = -f^{\perp}_{p_{-1}s}(\theta, \pi - \phi)$, and so does from equation (2.12) the vanishing of the sp_0 differential cross section in the xy plane ($\phi = 0, \pi$), $f^{\perp}_{p_0s}(\theta, 0/\pi) = 0$.

Note that calculations of differential cross sections for s-p excitation and capture have recently been performed for the one-electron collision system proton-H(1s), antiproton-H(1s), and He^{2+}-H(1s) (Hansen *et al* 1992). Special attention was given to heavy-particle interference effects and the validity of propensity rules for orientation in small-angle differential scattering.

Finally we shall give the amplitude expressions for channels from initially oriented p states of the target into oriented final p states on the projectile. In terms of the $T_f^{(l)}(\theta)$ functions defined above, equation (2.13), we obtain the scattering amplitudes for initial and final p states as

$$f^{\perp}_{p_{\pm1}p_{+1}}(\theta, \phi) = \tfrac{1}{2}[\mp T^{(p_0)}_{p_0}(\theta) - T^{(p_1)}_{p_1}(\theta) - \sqrt{2}(T^{(p_0)}_{p_1}(\theta) \mp T^{(p_1)}_{p_0}(\theta)) \cos\phi - T^{(p_1)}_{p_{-1}}(\theta) \cos 2\phi] \tag{2.14a}$$

$$f^{\perp}_{p_{\pm1}p_{-1}}(\theta, \phi) = \tfrac{1}{2}[\pm T^{(p_0)}_{p_0}(\theta) - T^{(p_1)}_{p_1}(\theta) - \sqrt{2}(-T^{(p_0)}_{p_1}(\theta) \mp T^{(p_1)}_{p_0}(\theta)) \cos\phi - T^{(p_1)}_{p_{-1}}(\theta) \cos 2\phi] \tag{2.14b}$$

$$f^{\perp}_{p_0p_{\pm1}}(\theta, \phi) = \pm i T^{(p_0)}_{p_1}(\theta) \sin\phi + \frac{i}{\sqrt{2}} T^{(p_1)}_{p_{-1}}(\theta) \sin 2\phi \tag{2.15a}$$

$$f^{\perp}_{p_0p_0}(\theta, \phi) = -T^{(p_1)}_{p_1}(\theta) + T^{(p_1)}_{p_{-1}}(\theta) \cos 2\phi. \tag{2.15b}$$

We observe the following left-hand/right-hand differential asymmetry relations for the oriented states, $f^{\perp}_{p_{+1}p_{+1}}(\theta, \phi) = f^{\perp}_{p_{-1}p_{-1}}(\theta, \pi - \phi)$ and $f^{\perp}_{p_{+1}p_{-1}}(\theta, \phi) = f^{\perp}_{p_{-1}p_{+1}}(\theta, \pi - \phi)$ as well as the vanishing of the $p_{\pm1} \to p_0$ differential cross sections in the (xy) plane ($\phi = 0, \phi = \pi$), $f^{\perp}_{p_0p_{\pm1}}(\theta, 0/\pi) = 0$.

2.3. The semiclassical model of H^+-Na collisions

The Schrödinger equation is solved using the impact parameter method within the straight line, constant velocity approximation. The scattering state is expanded on a basis set of travelling atomic orbitals centred on both nuclei. The Na(nl) states have been obtained by solving numerically the Schrödinger equation using the frozen core model potential

$$V(r) = -1/r - (17.9635 + 10/r)\, e^{-3.5927r} \tag{2.16}$$

optimized to give the proper ground state ionization potential. The states are then fitted with combinations of Slater orbitals and the results are given in table 1. In the present paper most of the solutions have been obtained in a basis of 19 separated atomic states, including the $n = 1$ and 2 shells and the 3s, 3p states in hydrogen, the $n = 3$ shell and the 4s state in sodium. We present also results at 3 keV proton energy obtained with a larger basis of 33 atomic states in which H(3d, 4s) and Na(4p, 4d) are added. The two-centre and one-centre matrix elements between these states are computed on a narrow grid of 350 mesh points on average and the coupled equations are integrated as far as $Z_0 = 150$ au to ensure reasonable convergence of the amplitudes. The probability amplitudes are computed for 172 impact parameters to ensure accurate evaluation of the eikonal integrals.

Table 1. Energies ε_{nl} (au) and parameters for the analytical fits to the radial part of the orbitals for Na nl states, $R_{nl}(r) = \Sigma_i c_i r^{n_i} e^{-\alpha_i r}$.

State	ε_{nl}		Coefficients						
3s	−0.1891	c_i	2.0949	−13.822	0.264 64	0.025 567			
		α_i	3.60	4.50	0.950	0.650			
		n_i	0	1	2	2			
3p	−0.1115	c_i	3.7781	−0.148 74					
		α_i	3.80	0.440					
		n_i	1	1					
3d	−0.0556	c_i	0.009 0793						
		α_i	0.334						
		n_i	2						
4s	−0.0717	c_i	0.637 54	−4.1113	−0.217 87	0.0217 814	3.6212	0.191 90	−0.019 214
		α_i	2.60	2.60	0.850	0.377	2.60	0.850	0.377
		n_i	0	1	1	1	2	2	2
4p	−0.0504	c_i	0.090 304	−0.007 0324	−0.093 841	0.007 3078			
		α_i	0.670	0.290	0.670	0.290			
		n_i	1	1	2	2			
4d	−0.0313	c_i	0.010 781	−0.003 4566					
		α_i	0.300	0.205					
		n_i	2	2					

3. Results

3.1. Total cross sections

As a first step of the investigation which also provides a good test of our collision model we have computed H($n = 2$) total capture cross sections using

$$\sigma_{nl}^{(i)} = 2\pi \sum_m \int_0^\infty b \, db |c_{nlm}^{(i)}(b)|^2 \tag{3.1}$$

for H^+–Na(3s) and aligned H^+–Na(3p) collisions in the intermediate energy range 0.75–5.0 keV. In table 2 they are compared with results of other atomic-basis calculations (b, c) and molecular-basis calculations (d, e). Results from measurements of L_α emission cross sections are given in f. Note that these latter ones should be compared to theoretical results after inclusion of cascade effects, which are, however, reported by Gieler *et al* (1991) to be no larger than 10%.

Good agreement is found between the present work and the calculations of Fritsch (1990) and Shingal and Bransden (1987). The comparison with molecular calculations, although less satisfactory, seems to indicate that our atomic state description is very reasonable in this intermediate energy range. To test our basis set dependence, results from 33-state calculations at 3 keV are also listed in table 2. It is found that the increase of the basis size changes the results by less than 20% and tends to improve agreement with those of Fritsch (1990). They also compare well with earlier results of Dubois *et al* (1991). It is expected that inclusion of ionization channels should not be of great importance for the H($n = 2$) cross sections in this energy range (Fritsch 1987).

In agreement with the experiments of Royer *et al* (1988), our results predict a preference for capture from the initial excited state in this energy range. Another interesting comparison is provided by the experimental study of Richter *et al* (1990)

Table 2. Total cross sections (in 10^{-16} cm^2) at six different projectile energies for H(2s) and H(2p) capture from three different initial states Na(3s), Na($3p_\sigma$) and Na($3p_\pi$): a, present work (19 states), a[1] (33 states); b, from Fritsch (1990) (49 states) b[1] at 1.7 keV; c, from Shingal and Bransden (1987) (34 states) c[1] at 0.8 keV, c[2] at 1.6 keV; d, from Courbin *et al* (1990) (19 states); e, from Allan *et al* (1986) e[1] molecular, e[2] atomic calculations; f, from Gieler *et al* (1991) experimental data (L_α emission cross section) f[1] at 0.7 keV.

		from	3s		$3p_\sigma$		$3p_\pi$	
E (keV)	v (au)	to	2s	2p	2s	2p	2s	2p
		a	6.6	13.5	10.1	87.7	5.1	52.4
0.75	0.173	c[1]	9.2	17.1				
		f[1]		15.7				
		a	8.8	17.2	10.8	85.8	4.3	52.2
1.00	0.200	b	10.1	17.9	9.2	72.0	4.5	51.4
		c	12.2	17.4				
		d	15.6	19.5	21.8	64.2	10.7	57.4
		e[1]		20.8		67.7		59.9
		e[2]		20.6		68.5		50.5
		f		18.3				
		a	14.5	23.7	17.3	71.4	3.3	48.8
1.50	0.245	b[1]	16.7	21.1	17.0	57.8	2.8	50.0
		c[2]	15.8	20.7				
		d	17.3	21.9	26.6	49.6	8.9	56.7
		f		20.7				
		a	22.6	29.9	19.1	60.3	2.6	42.8
2.00	0.283	c	18.9	25.8				
		d	18.0	25.9	28.2	42.0	7.6	54.1
		f		25.3				
		a	28.2	35.3	13.6	47.1	1.6	30.8
3.00	0.350	a[1]	22.9	27.9	14.7	45.9	2.1	34.2
		b	23.5	32.8	14.0	44.1	2.4	38.4
		c	22.1	34.5				
		d	17.9	34.2	26.8	36.9	6.2	49.3
		f		36.4				
		a	20.7	29.0	5.7	33.2	0.8	16.1
5.00	0.447	b	17.4	31.3	3.6	30.7	1.9	21.6
		c	17.2	31.8				
		d	15.6	37.1	18.8	33.1	4.6	41.3
		f		32.2				

on effects of initial orbital alignment on H^+-Na(3p) collisions. They measure the cross section ratios $\sigma_{3p_\sigma \to n=2}/\sigma_{3s \to n=2}$ and $\sigma_{3p_\pi \to n=2}/\sigma_{3s \to n=2}$ by controlling the polarization of the laser light used for initial excitation. For these two parameters we find at 1 keV: 3.7 and 2.2 respectively (2 keV: 1.5 and 0.9) in excellent agreement with their results 3.3 ± 0.35 and 2.3 ± 0.25 (2 keV: 1.6 ± 0.15 and 1.15 ± 0.1). The same weak dependence upon energy for the asymmetry parameter $A(n=2) = (\sigma_{3p_\sigma \to n=2} - \sigma_{3p_\pi \to n=2})/(\sigma_{3p_\sigma \to n=2} + \sigma_{3p_\pi \to n=2})$ is also confirmed with a value of 0.26 (0.16 for Richter *et al* 1990). The $A(n=3)$ parameter from our calculations presents the same dramatic decrease with energy as obtained by Richter *et al* (1990), but slightly shifted towards higher energies.

In conclusion comparisons with available theoretical and experimental studies at the level of total cross sections are very satisfactory and give confidence in our model in the energy range under consideration.

3.2. Differential cross sections

A more sensitive level of comparison is provided by the differential cross sections (DCS)

$$\frac{d\sigma_f^{(+)}}{d\Omega} = \frac{v_f}{v_i} |f_{fi}^{\perp}(\theta, \phi)|^2. \tag{3.2}$$

In the following both DCS and scattering angles will refer to the laboratory system and the states will be those referred to the *xyz* reference frame of figure 1, cf section 2.2.

We first focus on capture from the Na(3s) ground state, the simplest case to analyse from the point of view of final orientation. Then we analyse $H(n=2)$ capture from the Na(3p) states, and finally the $Na(3p_{\pm 1}) \rightarrow H(3p_{\pm 1})$ transitions in the 33-state basis.

3.2.1. H^+-Na(3s) collisions. In figure 2 (top panel) are shown for different channels at 1 keV (*a*) the results sin θ times differential cross section as a function of laboratory scattering angle θ for an azimuthal angle $\phi = 0$ (left-hand side scattering) and (*b*), for comparison, the impact parameter results $b \times |c_f^{(3s)}|^2$ as a function of b for a classical left-hand side proton trajectory.

A general interpretation of the shape of the DCS is most clearly provided by the analysis of the $Na(3s) \rightarrow H(2s)$ transition. Indeed the scattering amplitude integral has a simple Fraunhofer expression

$$f_{2s3s}^{\perp}(\theta, \phi) = -i\mu v \int_0^{\infty} db\, b c_{2s}^{(3s)}(b) J_0(2\mu v \sin(\theta/2) b) \tag{3.3}$$

where the contribution of each factor can readily be evaluated. The modulus of $b \times c_{2s}^{(3s)}$ presents a clear maximum at $b \approx 10$ au (cf figure 2(*b*) top panel). Furthermore, for $b \approx 8$-17 au, the phase of the amplitude $c_{2s}^{(3s)}$ varies little so that the main contribution to the integral clearly comes from this range. On the other hand, the Bessel function whose argument is approximately equal to $\mu v \theta b$ can be expressed as a series

$$J_0(\mu v \theta b) = 1 - (\tfrac{1}{2}\mu v \theta b)^2 + \tfrac{1}{2}(\tfrac{1}{2}\mu v \theta b)^4 - \tfrac{1}{6}(\tfrac{1}{2}\mu v \theta b)^6 + \ldots. \tag{3.4}$$

For small scattering angles (e.g. 0.01°), the second-order term can contribute only when b is large and the first node of the J_0 function is thus far outside the important range of integration and the DCS is maximum. For increasing θ, the second-order term may give rise to cancellation for smaller b: for example at $\theta = 0.035°$, $1 - (\frac{1}{2}\mu v \theta b)^2 \approx 0$ for $b \approx 10$ au, just at the maximum of $|c_{2s}^{(3s)}|$, i.e. results in a minimum of the DCS. For even larger θ, the higher order nodes move into the important range of b and, depending upon their locations with respect to the peak, the DCS presents a damped oscillatory behaviour. For $\theta \approx 0.06°$, the first nodes are at 7 and 17 au and affect only weakly the total integral. In general the origin of the oscillatory behaviour of the DCS is less clear due to a broader probability peak and phase effects interfering with the cancellations of the Bessel function.

Let us now focus on the orientation of the final 2p capture state, again at 1 keV energy. It has been shown by Nielsen *et al* (1990) and confirmed recently by Dubois

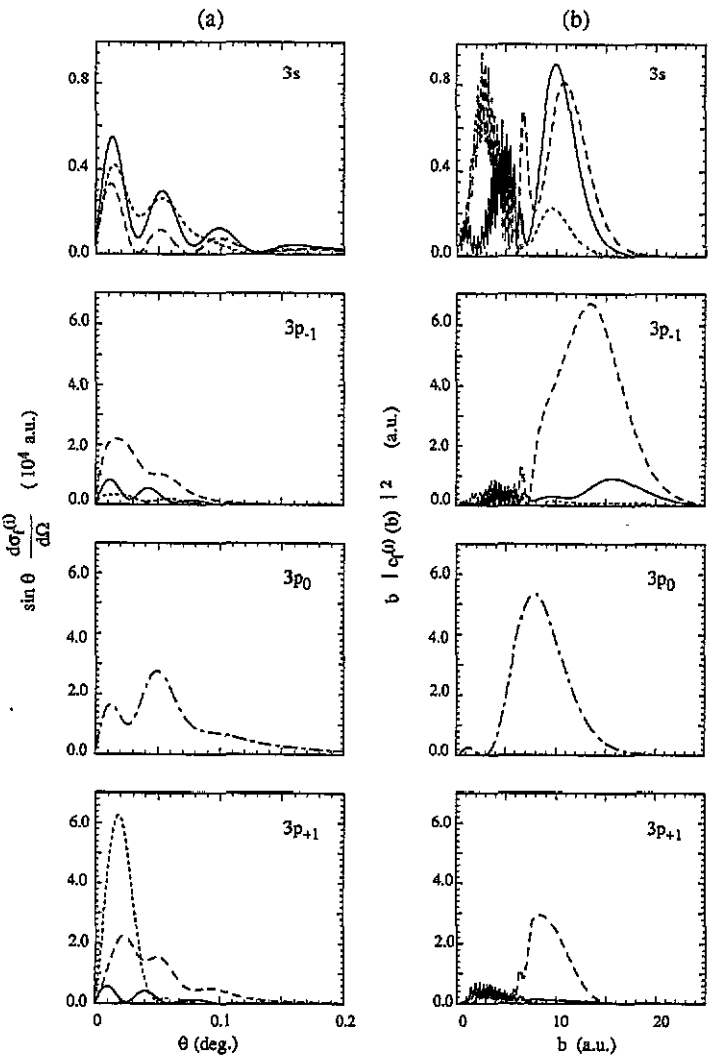

Figure 2. (*a*) $\sin(\theta)\, d\sigma_f^{(i)}(\theta, 0)/d\Omega$ (left-hand side differential cross sections) as functions of laboratory scattering angle θ and (*b*) $b|c_f^{(i)}|^2$ (left-side hand collision probabilities) as function of impact parameter b, for 2s (full curve), $2p_{-1}$ (long-dashed broken curve), $2p_0$ (chain curve) and $2p_{+1}$ (short-dashed broken curve) capture states at impact energy $E = 1.0$ keV. The panels from top to bottom correspond to initial 3s, $3p_{-1}$, $3p_0$ and $3p_{+1}$ states respectively, all states quantized (oriented) in the *xyz* frame, from 19-state close coupling calculations.

et al (1991) that in an impact parameter description these endoergic channels ($\Delta\varepsilon \approx 0.064$ au) will preferentially populate the $2p_{-1}$ state in a left-hand trajectory calculation. This is in agreement with the propensity rules for orientation derived for excitation by Andersen and Nielsen (1987). Figure 2(*b*) (top panel) shows indeed a clear preference for the $2p_{-1}$ state over the most important impact parameter range. However for left-hand side scattering, capture to the $2p_{+1}$ state is the dominant channel, from 0.02° up to 0.1°: the orientation propensity in differential results is thus reversed and less pronounced. The last feature may be explained by the fact that many impact parameters contribute to each θ so that the clear *b*-picture is smeared out by the

integration. The reversion is less obvious to explain. It can be shown (Hansen *et al* 1992) that the s–$p_{\pm 1}$ scattering amplitudes, for $\eta b > 1$ (in our case ≈ 3), may be expressed as a sum of two b integrals corresponding to left-hand side and right-hand side trajectories. A stationary phase argument can then determine which trajectories are the more important for a given (θ, ϕ) detection geometry. For capture in doubly and multiply charged ion–atom collisions, the contribution to the b-dependent phases of the amplitudes from the asymptotic Coulombic interaction allows a clear stationary phase prediction of orientation propensity. For singly charged systems there is no such phase contribution and a definite stationary phase result is less certain. With an effective repulsive scattering potential we expect the left-hand side classical trajectories to dominate the left-hand side scattering ($\phi = 0$), but with an attractive potential, however, to dominate the right-hand side scattering ($\phi = \pi$). The 3s–$2p_{\pm 1}$ capture results of figure 2 (upper panel) thus suggest that an atractive potential is effectively responsible for the deflection. This is reasonable when the process happens at relatively large impact parameters where the usual ion-induced dipole interaction potential $-a/R^4$ is expected to be approximately correct.

For vanishing scattering angles however, the DCSs for capture from 3s to the $2p_{\pm 1}$ states become identical. In this case ($\eta b \approx 0.3$) the previous argument does not hold and one can predict this behaviour from the expressions for $f^{\perp}_{p_{\pm 1}s}$ given in equation (2.11b). In the limit $\eta b \to 0$, $J_1(\eta b) \to 0$ while $J_0(\eta b) \to 1$: the first term becomes dominant and the two amplitudes differ only by a trivial phase. In other words, in this range of scattering angles, strong quantal interferences between trajectories can be seen: right- and left-hand side trajectories contribute and orientation effects seen in the b picture disappear. This is observed in figure 2(a) (upper panel) for $\theta < 0.02°$.

For higher impact energies propensity rules for the endoergic Na(3s) → H(2p) capture are again observed in the classical trajectory results (figures 3(b) and 4(b) upper panels). At the probability maxima we see very clear dominance of capture to the $2p_{-1}$ state. For these higher energies the resulting differential cross sections show an expected enhancement in the forward direction. The orientation effect is here nearly completely absent over the important scattering angle range ($\theta < 0.02°$), a result following from quantal interferences as mentioned above.

3.2.2. H^+–Na(3p) collisions. First of all, it is worth noting the very different H(2s/2p) balance for initial Na(3p) compared with initial Na(3) states: while, for capture from Na(3s), the H(2s) and H(2p) states are at equal footing, the capture to H(2p) strongly dominates the H($n = 2$) capture channels in H^+–Na(3p) collisions.

The orientation effects in the $Na(3p_{\pm 1}) \to H(2p_{\pm 1})$ capture channels are difficult to interpret in terms of the propensity rule criterion of Andersen and Nielsen (1987). The transition is exoergic with a small energy change ($\Delta\varepsilon \approx -0.014$ au) and the criterion would predict propensity for orientation corresponding to increasing magnetic quantum number. However as already discussed by Nielsen *et al* (1990), this criterion is not formally valid for capture, especially when involving near-resonant states, for which the transitions may become effectively endoergic at higher velocities due to the additional kinetic energy of the electron captured by the projectile ion.

The second and fourth panels of figure 2(b) do show this tendency. From an initial $Na(3p_{-1})$ state the $H(2p_{+1})$ state is hardly populated compared to significant $H(2p_{-1})$ capture, while from $Na(3p_{+1})$ capture to $H(2p_{-1})$ is preferred. This behaviour can be understood rather by the 'velocity matching' concept discussed for p–p resonant capture by Campbell *et al* (1991) and references therein. This classical argument is based on

the fact that capture is favoured when the velocity of the projectile and that of the active electron are identical in magnitude and direction. In our case of a left-hand trajectory, capture from the $Na(3p_{-1})$ state is the dominant channel beyond an impact parameter corresponding to the velocity matching and then the $H(2p_{-1})$ is favoured. This argument is well illustrated in figure 2 of Campbell *et al* (1991). In contrast, capture from $Na(3p_{+1})$ to $H(2p_{+1})$ is nearly completely suppressed in left-hand trajectories.

The angular differential results in figure 2(*a*) reflect this more intricate picture. Comparison between the $Na(3p_m) \rightarrow H(2p_m)$ capture probabilities in the trajectory description (figure 2(*b*) shows the left-hand passages of the projectile) and the differential capture cross sections for left-side ($\phi = 0$) scattering (figure 2(*a*)), allow the following conclusions.

(i) For an H^+ flux against an initial $Na(3p_{+1})$ oriented state we find for left-hand side scattering a dominant, large $H(2p_{+1})$ capture cross section for small θ ($<0.04°$), and a dominant, but medium sized $H(2p_{-1})$ capture cross section for larger θ. This implies that an effective attractive potential is responsible for $Na(3p_{+1}) \rightarrow H(2p)$ capture scattering at large b (right-hand trajectories give large $p_{+1} \rightarrow p_{+1}$ capture probabilities), and that an effective repulsive potential is dominating at smaller b (left-hand trajectories give moderate $p_{+1} \rightarrow p_{-1}$ capture probabilities).

(ii) For an H^+ flux against an initial $Na(3p_{-1})$ oriented state we find for left-hand side scattering ($\phi = 0$) a dominant but medium sized $H(2p_{-1})$ capture cross section at all θ. This seems to imply that in this case an interplay between attractive and repulsive potential terms results in a modest overall dominance of the repulsive trajectories, as indicated by the large $p_{-1} \rightarrow p_{-1}$ capture probabilities for left-hand trajectories against the smaller $p_{-1} \rightarrow p_{+1}$ probabilities for right-hand trajectories.

Quantal phases are also very important and, again, no one-to-one equivalence can be derived formally between differential and semiclassical results. For the smallest scattering angles, in contrast to figure 2(*a*) top panel, orientation effects are still observable. Indeed, in this range, two terms in equation (2.14) ($T_{p_0}^{(p_0)}$, $T_{p_1}^{(p_1)}$) are dominant and give rise to this asymmetry. This also explains the convergence seen for $\theta \rightarrow 0$ of the DCS for the $Na(3p_{-1}) \rightarrow H(2p_{-1})$ and $Na(3p_{+1}) \rightarrow H(2p_{+1})$ channels, likewise for $Na(3p_{-1}) \rightarrow H(2p_{+1})$ and $Na(3p_{+1}) \rightarrow H(2p_{-1})$.

The results at 3 and 5 keV (figures 3 and 4) show very analogous behaviour in b dependence, with only slight shifts to lower impact parameters and smaller scattering angles. In differential cross sections, the orientation asymmetries survive and seem only weakly dependent upon velocity in this range. Finally note that we also present in figures 2, 3 and 4 capture results for the aligned states, $Na(3p_0) \rightarrow H(2p_0)$. At all energies the b-dependence presents a clear maximum at somewhat lower impact parameters than for $Na(3p_{\pm 1})$, as would be expected from geometrical considerations. The corresponding DCS therefore extend to larger angles and have still not vanished at 0.2°. Differential measurements of $H(n=2)$ capture from a hybrid Na(3p) initial state will therefore be dominated by these transitions at larger scattering angles. This behaviour is in agreement with the scattering angle dependence of the coherence parameter h displayed in figure 8 of the companion paper (Richter *et al* 1993).

3.2.3. Thirty-three-state calculations. It is instructive to compare differential cross sections evaluated with a different size of basis sets, cf section 3.1. In figure 5 we present the probabilities and the differential cross sections at 3 keV for total $H(n=2)$ capture from Na(3s) and $Na(3p_m)$ initial states, obtained by 19- and 33-state calculations. The

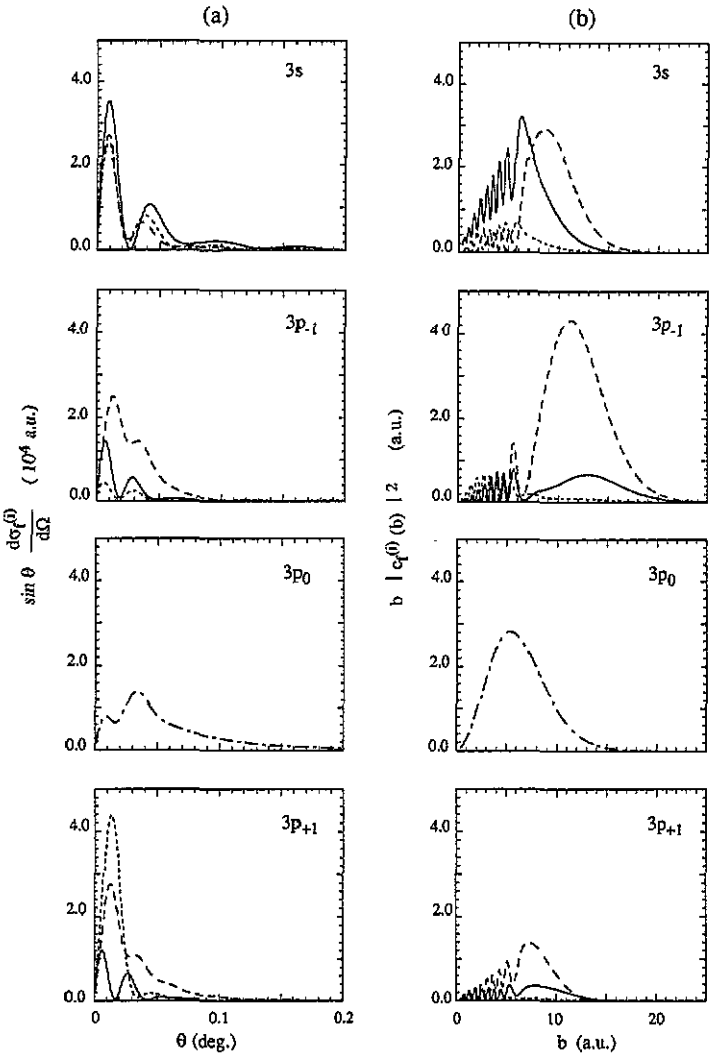

Figure 3. Same as figure 2 for $E = 3.0$ keV.

most important changes are observed for H^+-Na(3s) collisions at intermediate impact parameters. However as can be seen from figure 5(a) the results seem to be well converged. Especially it is gratifying to observe the near-identical angular dependence.

The 33-state calculation at 3 keV allows us to predict orientation effects also for endoergic capture from Na(3p) to the H(3p) states. It may eventually become possible to do such measurements for these higher energies for which the cross sections become nearly as large as the ones for H(2p) capture (Royer *et al* 1988, Donnelly *et al* 1991). In figure 6 DCS for $H(3p_{\pm 1})$ capture from $Na(3p_{+1})$ are presented for $\phi = 0$ and $\phi = \pi$. Dominance of capture to $H(3p_{-1})$ states is observed for left-hand side scattering ($\phi = 0$) up to 0.1°, while $H(3p_{+1})$ is preferred to the right-hand side ($\phi = \pi$). These orientation effects are more clear than those predicted for H(2p) capture (figure 3). The differential measurements are complicated to perform at these small angles. Note, however, that it should become possible to observe dominance of $Na(3p_{+1}) \rightarrow H(3p_{-1})$ over $Na(3p_{+1}) \rightarrow H(3p_{+1})$ at the level of total cross sections. The difference can be seen from

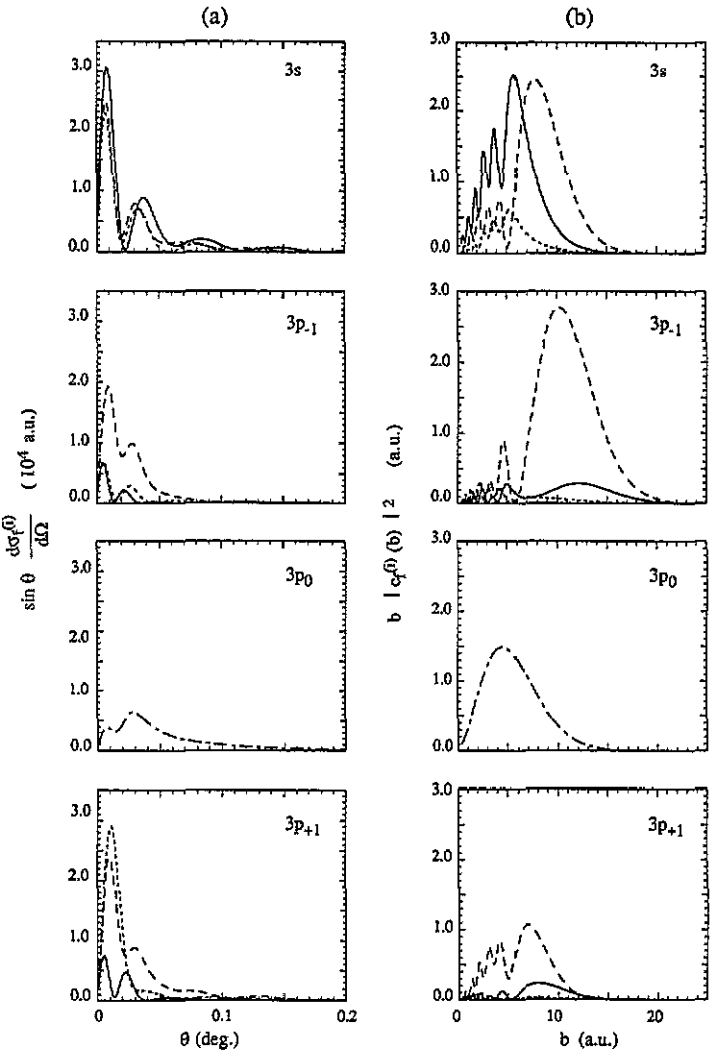

Figure 4. Same as figure 2 for $E = 5.0$ keV.

equation (2.14) after squaring and integrating over ϕ. We find differences of about 15% between the total cross sections for these two channels (compared to only 5% for $Na(3p_{+1}) \rightarrow H(2p_{\pm 1})$). Such experimental studies have not been performed and will represent yet another level of investigation.

4. Comments and conclusion

We have derived explicit expressions for scattering amplitudes for oriented states quantized perpendicular to the projectile beam axis. The theory is applied to a study of orientation effects for initial and final s and p states in H^+-Na capture collisions in the intermediate energy range. We have seen that orientation effects at small angles cannot be interpreted using only the semiclassical picture. The eikonal transforms for

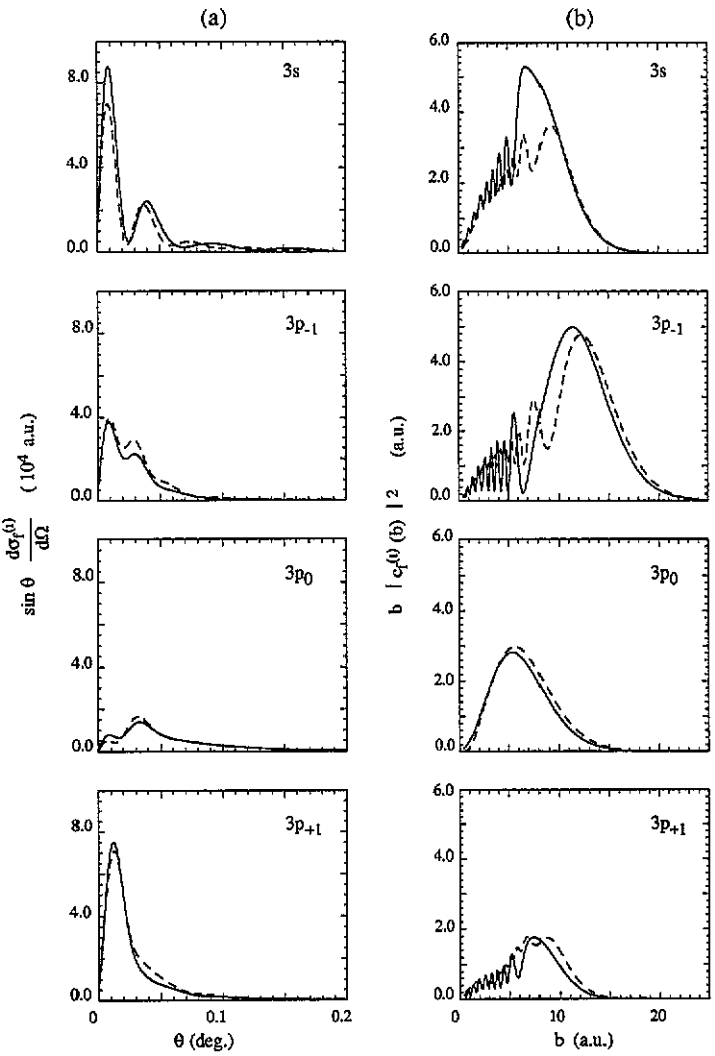

Figure 5. Same as figure 2 for $E = 3.0$ keV, except that the full and broken curve now show the complete H($n = 2$) capture shell results from 19-state and 33-state calculations, respectively.

the scattering amplitudes, although relatively simple for these transitions, present a quite complicated interplay of many factors. Whereas results at larger scattering angles may be understood in terms of effective interactions governing the scattering, as used e.g. for s-$p_{\pm 1}$ excitation in the classical rolling ball concept (Hertel *et al* 1985), the small scattering angle range displays the collapse of the classical trajectory picture due to quantal interferences between trajectories. A discussion of these aspects of differential scattering events can be found in Hansen *et al* (1992).

The present atomic basis close-coupling results in combination with the eikonal method, give excellent agreement with recent experimental capture results presented in a companion article (Richter *et al* 1993). Measurements confirm quantitatively both angular differential cross sections and the left/right orientation asymmetries predicted in the present work. Initial alignment effects are also presented in Richter *et al* (1993)

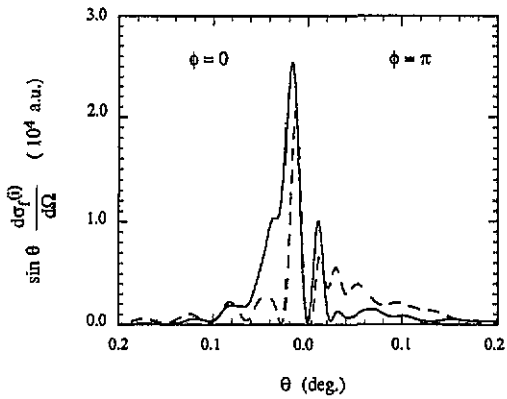

Figure 6. $\sin(\theta) \times d\sigma_f^{(1)}(\theta, 0)/d\Omega$ as functions of laboratory scattering angle θ for H(3p) capture in 3.0 keV H^+–$Na(3p_{+1})$ collisions. The full and broken curves correspond to final oriented $H(3p_{-1})$ and $H(3p_{+1})$ states respectively. The $\phi = 0$ part corresponds to left-hand side detection, the $\varphi = \pi$ part to right-hand side detection of the projectile.

and compared with the predictions of our calculations (not displayed in the present paper).

New experimental investigations of this collision system are proposed and commented on. Preparation of a specific magnetic initial state followed by angular momentum analysis of the final capture state can provide, at the level of differential as well as integral cross sections, a further level of sophistication in the study of the scattering dynamics.

Reports of related experimental and theoretical studies concerning orientation effects for capture in multiply-charged ion–atom collisions, for which strong Coulombic repulsion dominates the scattering events, are forthcoming (Adjouri *et al* 1993).

Acknowledgments

This work has been supported by the Danish Natural Science Council, the Norwegian Research Council and NorFA. Parts of the computations have been performed with the support of Conseil Scientifique du Centre de Calcul Vectoriel pour la Recherche.

References

Adjouri C, Barat M, Roncin P, Andersen N, Hansen J P, Nielsen S E and Dubois A 1993 in preparation
Allan R J, Courbin C, Salas P and Wahnon P 1990 *J. Phys. B: At. Mol. Opt. Phys.* **23** L461
Allan R J, Shingal R and Flower D R 1986 *J. Phys. B: At. Mol. Phys.* **19** L251
Andersen N, Gallagher J W and Hertel I V 1988 *Phys. Rep.* **165** 1
Andersen N and Nielsen S E 1987 *Z. Phys.* D **5** 309
Aumayr F, Lakits G and Winter H 1987 *J. Phys. B: At. Mol. Phys.* **20** 2025
Berkowitz J K and Zorn J C 1984 *Phys. Rev.* A **29** 611
Briggs J S and Macek J H 1990 *Adv. At. Mol. Opt. Phys.* **28** 1
Campbell E E B, Hertel I V and Nielsen S E 1991 *J. Phys. B: At. Mol. Opt. Phys.* **24** 3825
Campbell E E B, Schmidt H and Hertel I V 1988 *Adv. Chem. Phys.* **72** 37
Courbin C, Allan R J, Salas P and Wahnon P 1990 *J. Phys. B: At. Mol. Opt. Phys.* **23** 3909
Donnelly A, Geddes J and Gilbody H B 1991 *J. Phys. B: At. Mol. Opt. Phys.* **24** 165
Dowek D, Houver J C, Pommier J, Richter C, Royer T, Andersen N and Palsdottir B 1990 *Phys. Rev. Lett.* **64** 1713
Dubois A, Hansen J P, Lundsgaard M and Nielsen S E 1991 *J. Phys. B: At. Mol. Opt. Phys.* **24** L269

Finck K, Wang Y, Roller-Lutz Z and Lutz H O 1988 *Phys. Rev.* A **38** 6115
Flannery M R and McCann K J 1973 *Phys. Rev* A **8** 2915
Fritsch W 1984 *Phys. Rev.* A **30** 1135
—— 1987 *Phys. Rev.* A **35** 2342
—— 1990 private communication to D Dowek
Gieler M, Aumayr F, Ziegelwanger P, Winter H and Fritsch W 1991 *Phys. Rev.* A **43** 127
Hansen J P, Nielsen S E and Dubois A 1992 *Phys. Rev.* A **46** 5331
Hertel I V, Schmidt H, Bähring A and Meyer E 1985 *Rep. Prog. Phys.* **48** 375
Houver J C, Dowek D, Richter C and Andersen N 1992 *Phys. Rev. Lett.* **68** 162
McCarroll R 1982 *Atomic and Molecular Collision Theory* NATO ASI Series B ed F A Gianturco (New York: Plenum) p 165
McCarroll R and Salin A 1968 *J. Phys. B: At. Mol. Phys.* **1** 163
Lewartowski E and Courbin C 1992 *J. Phys. B: At. Mol. Opt. Phys.* **25** L63
Nielsen S E, Hansen J P and Dubois A 1990 *J. Phys. B: At. Mol. Opt. Phys.* **23** 2595
Piacentini R D and Salin A 1977 *Comput. Phys. Commun.* **13** 57
Richter C, Dowek D, Houver J C and Andersen N 1990 *J. Phys. B: At. Mol. Opt. Phys.* **23** 3925
Richter C, Andersen N, Brenot J C, Dowek D, Houver J C, Salgado J and Thomsen J 1993 *J. Phys. B: At. Mol. Opt. Phys.* **26** 723–43
Roller-Lutz Z, Finck K, Wang Y and Lutz H O 1991 Private communication
Royer T, Dowek D, Houver J C, Pommier J and Andersen N 1988 *Z. Phys.* D **10** 45
Shingal R and Bransden B H 1987 *J. Phys. B: At. Mol. Phys.* **20** 4815
Wilets L and Wallace S J 1968 *Phys. Rev.* **169** 84